Monitoring of Urmia Lake Bridge Subsidence during 2014- 2021 Using DInSAR-SBAS Method and GPS Data

F. Zamiri-Aghdam[1], M. Akhoondzadeh*[1], M. Dehghanijabbarlou[2]

[1]School of Surveying and Geospatial Engineering, College of Engineering, University of Tehran, Tehran
{aghdam.zamiri.fa, *makhonz}@ut.ac.ir

[2]Institute of Earth and Space Sciences, Eskisehir Technical University, Turkey
miladdehghanijabbarlou@eskisehir.edu.tr

Abstract

The Differential Interferometric Synthetic Aperture Radar (DInSAR) can be considered an efficient and cost-effective method for monitoring ground subsidence because of its extensive spatial coverage and high precision. Because of orderly observations from a broad-range product, the new commissioning of the first Sentinel-1 satellite offers better support to operational scrutinies via DInSAR. In the present paper, the results of a Small Baseline Subset Interferometric Synthetic Aperture Radar (SBAS-InSAR) time-series analysis of 42 Interferometric Wide swath (IW) products of Urmia Lake Bridge in northwestern Iran acquired between November 2014 to April 2021 for both descending and ascending pass using the Sentinel-1A observation with Progressive Scans in azimuth (TOPS) imaging mode is studied. The SBAS processing was based upon the analysis of 111 small-baseline differential interferograms. The results demonstrate that the majority of regional ground subsidence rates in the research area ranged from 10 to 210 mm during the study period. Also, the maximum subsidence rate exceeded 210 mm/year. The Line of Sight (LOS) direction for descending pass is 91 mm/year for ascending the pass. The board view displays that ground subsidence is intense on the bridge. The largest subsidence center is located at the central points of the bridge. GPS data verified the SBAS-InSAR-derived result. The results include displacement in the horizontal and vertical directions for ascending and descending passes.

---

* Corresponding Author

1. Introduction

Surface subsidence is one of the world's most important engineering geological issues and is caused, for example, by natural earthquakes [1] or human-causing activities such as groundwater extraction and underground construction [2]; [3] Surface subsidence is also one of the biggest regional geological disasters causing significant damage to buildings, infrastructure, roads and bridges, and human security in urban areas. [4];[5];[6], Ground subsidence can be mapped with high precision. Utilizing satellite-based methods, the most prevalent is differential interferometric synthetic aperture radar (DInSAR). The interferometric Synthetic Aperture Radar (InSAR) has been frequently employed to analyze surface subsidence [7]. It was impossible to monitor the deformation of areas developed by groundwater using techniques such as leveling and GPS. However, the InSAR method, with high accuracy of hardly any millimeters to a few centimeters, a high spatial resolution of 102 square meters, and high coverage of the study areas, provided a suitable way to monitor and detect land deformation[8]. Compared to traditional monitoring methods such as the Global Navigation Satellite System (GNSS) [9]; [10], leveling [11], geological and geophysical investigation methods [12]. However, it is impossible to detect and analyze regional deformation across the entire city properly [10]; [9]. due to the distribution of monitoring results for GPS and leveling[13] methods is poor.

Differential InSAR (DInSAR) technology uses traditional InSAR technology to generate an interferogram containing surface deformation and terrain information from two radar images. It then inverts the terrain phase based on the external DEM and eliminates it from the interference phase [14]. Finally, an interferogram with solely topographical deformation information is acquired; however, the interferogram also has an atmospheric phase effect, making high-precision measurements problematic [15]. However, some problems limited the applications of SAR, including the variability of scatter properties over time and look direction and other problems like low temporal resolution, geometrical distortion, and a considerable distance between the sensor and monitored object [16];[17]. Therefore, in recent years, multi-time InSAR techniques (MT-InSAR) have been developed to retrieve long time series and overcome the mentioned problems. These advanced techniques with SAR dataset time series analysis present the result of high accuracy of deformation; these techniques include Persistent Scatterer Interferometry (PSI) [18], Small Baseline Subset Approach (SBAS) [19];[20], Coherent Pixels Technique(CPT) [21] and Interferometric Point Target Analysis (IPTA) [22]. SBAS and PS technologies are powerful multi-temporal tools for wide-area land deformation monitoring; however, their processing strategies are different. PSInSAR analyzes the amplitude and phase stability to explore a subset of image pixels corresponding to phase-stable privileged reflectors (e.g., buildings, bare rocks, corner reflectors, and so on.), which are not influenced by temporal-spatial baseline decorrelation. Unlike PSInSAR technology, which requires the targets to exhibit very high coherence values concerning the only single master image and assumes a constant velocity model for targets' motion, the SBAR technique makes unwrapping the interferogram easier and also to be able to analyze the time series of all pixels that are above the threshold. Selects interferograms that are very coherent and have short temporal and spatial baselines. [23]; [24]. Interferograms create a network to connect images in a spatial and temporal baseline space. Then Singular Value Decomposition (SVD) provides phase delay time series for inversing all sets of them and spatially unwrapping. The SBAS technique has several applications and advantages. This method makes it possible to study larger spaces, especially in non-urban areas, considering the SAR properties. [25].

Some other researchers that use the InSAR method or like that in their papers, for example [26], used the Advanced Land Observing Satellite (ALOS) Phased Array type L-band Synthetic Aperture Radar (PALSAR) DInSAR for the analysis of the surface displacement field of the 12 May 2008 magnitude 8.0 Wenchuan Earthquake. The advantage of the mentioned method is that it can be calculated without phase unwrapping. Compared to the original interferograms, the final mosaic of interferograms shows a significantly more consistent co-seismic surface-displacement field. On the other side [27], Subsidence in the southern part of the Delta was calculated using the PSI method of 0.4 mm/year using 84 ENVISAT SAR images between 2004 and 2010 over the entire Delta for their study. They also identified a 2.5 mm/year uplift in the central Delta. Finally, the highest subsidence rate in the province of Menoufia was calculated to be -9.7 mm/year [28] using 49 ENVISAT images obtained between 2003 and 2010 based on PSI calculated a subsidence rate of -0.4 to -2 mm/year. They thought that sediment density would overcome the ground subsidence on a shorter scale. At the same time, earthquakes and earth-building activities caused ground subsidence in the long run [29]. To monitor the displacement of Domus Tiberiana (Rome, Italy), terrestrial laser scanning and ground-based synthetic aperture radar interferometry from April 2009 to March 2010, they also evaluated the impact of human activity on the structure. In similar research, Deformation information was obtained considering white and color noise effects by combining ground-based

interferometric radar and Maximum License Estimate (MLE). The substances rate was −0.0122±0.0060 and −0.0065±0.0058 mm hour−1 for (No. 7 and No. 8). This results in the bridge being stable and secure[3]. [30] used a method for monitoring land deformation using SAR interferometry, and polarimetric information is given. A coherent target (CT)-neighborhood networking scheme can be utilized to attain the linear and nonlinear components of the deformation, the DEM error. Yearly rates of subsidence in the studied area range from -20 to 10 mm/year, with an average subsidence rate of -7.5 mm/year in the downtown area.

Most previous research had limited data or analyzed it over a short period, or did not evaluate the results of its InSAR method. The present paper collected data over seven years from the onset of the Sentinel 1A images production until 2021, with an interval of 4 months as well as ascending and descending crosses. The subsidence of Urmia Lake Bridge from November 2014 to April 2021 calculated using the SBAS method and evaluated the obtained results with GPS data of the station in the research area. For this purpose, displacement in vertical and horizontal directions validated for ascending and descending.

1. Methodology
1.1. Study area

Area of present research covers approximately 3650 square kilometers, including the Bridge of the Urmia Lake and the Urmia permanent GPS Station. This bridge is located in northwestern Iran. It connects East and West Azerbaijan provinces by crossing Lake Urmia and is Iran's largest and longest bridge. Figure 1 presents the location of the study area.

For this study, 42 Sentinel-1A IW SLC SAR used images obtained evenly in ascending and descending crossings from November 2014 to April 2021 with an interval of 4 months. With the incident angle of 39.16 degrees for descending cross and 43.83 degrees for ascending cross. All images used are in VV polarization mode, and Sentinel 1A images were taken from track 79 for descending path and from track 72 for ascending path. Images were downloaded from the Alaska Satellite Center. A topography map for descending crossings is demonstrated in Figure 1. In addition, the ASTER GDEM V2 worldwide elevation data (resolution 30 meters) used in the data processing process removes the terrain phase. The DEM data reflated and geocoded the resulting InSAR products from range-Doppler coordinates into map geometry conforming to the Universal Transverse Mercator (UTM) coordinate system. The raw data was processed, and time series analysis was performed using ENVI and SARscape software.
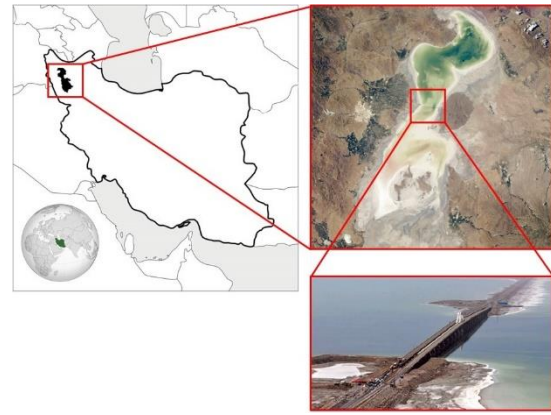

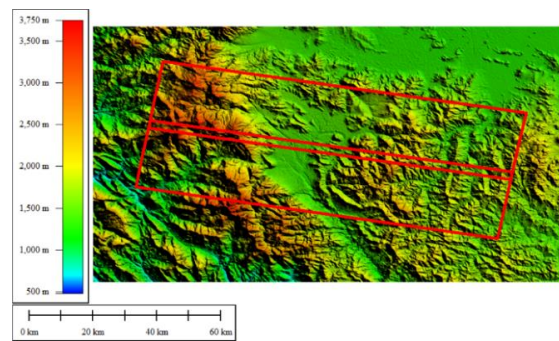Figure 1. Location of Lake Urmia in northwestern Iran

Figure 2. The coverage of the two bursts of Sentinal1A image

1.2. InSAR Dataset and Data Processing

SBAS-InSAR, a time series InSAR analysis approach, is a method that primarily entails the correlation arrangement and combination of several interferograms in small baselines, which is more resistant to decoherence, to improve the rate of temporary sampling. [31]; [32]; [33]. The SBAS-InSAR approach primarily utilizes the singular value decomposition method or the least-squares method to determine the deformation rate of the research area. To increment the rate of the sampling of the observation data, it can connect SAR datasets separated by a more excellent spatial baseline. In this paper, SARscape data processing software was used. The following are the main steps as shown in Figure 8 [34].

1.2.1. Image Coregistration and Resampling

During $(t_0, t_1, ..., t_n)$ time select an image as the super master image and register the remaining slave image. For each crossing, it was necessary to coregister the 21-slant range SLC images to a standard slant-range coordinate system once they were deburst and merged. For descending cross, The 18 October 2015, Sentinel-1 image was chosen as the super master (and for ascending cross on 17 October 2015), and the remaining 20 slave images were coregistered to the master separately, yielding 21 images in the master coordinate system. Only the amplitude data was used for matching in this step, and the coregistration method was a Fast Fourier Transform (FFT) [35].

1.2.2. Generation of the differential interferograms Differential

The SBAS method was used to create differential interferograms for short orbital baseline pairs of coregistered images is the same method that [36] and [37] used. All the formed pairs had a perpendicular baseline of no more than 250 meters. This low baseline threshold maximizes spatial coherence while reducing phase contribution caused by DEM inaccuracies [38].

Figure 3 demonstrates a plot of the perpendicular baseline and each acquisition time concerning the master image. Straight lines represent pairs that correspond to the baseline threshold. The whole number of interferograms generated for descending cross was 57, with an average absolute normal baseline of 29.64 meters and a mean absolute temporal baseline of 233 days. Moreover, for ascending cross, the number of pairs to analyze was 54, with a mean absolute normal baseline of 53.69 meters and a mean absolute temporal baseline of 224 days. Furthermore, the temporal baselines of these selected interferograms are demonstrated in Figure 4.

The differential interferograms were typically high quality, with outstanding coherence (average greater than 0.4) in several short temporal baselines. Because of the correction in the instrument data processing facility that was made to data processed after March 2015 and a difference in the elevation antenna pattern of scenes processed before and after March 2015, It was possible to introduce another phase discontinuity between the sub-swaths [39]. No correction was made for this inaccuracy because it was not visible in any interferograms generated here.
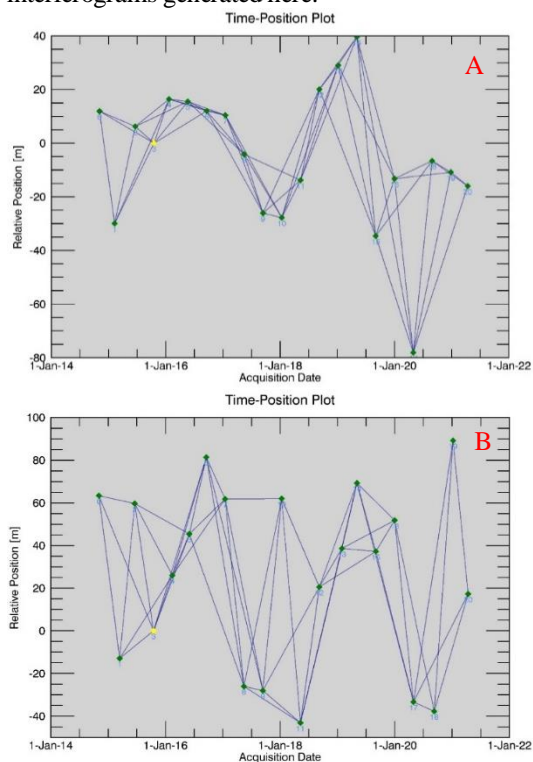

Figure 3. Perpendicular orbital baseline and time relative to the master, for descending on 18 October 2015 (A) and ascending on 17 October 2015 (B).

In Figure 3, The green points illustrate SAR images, Straight lines connecting two images show interferogram pairings, and the yellow dot denotes the super master image
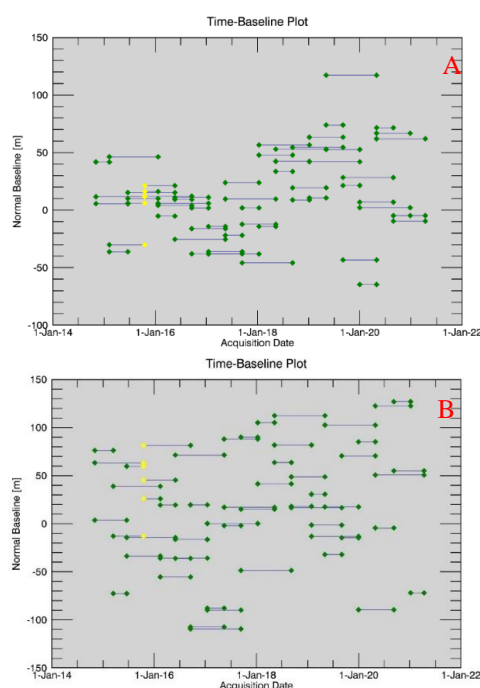

Figure 4. Time-baseline plots of the SAR images and interferograms of the 57 SAR acquisition dates for descending cross (A) and 54 for ascending cross (bottom).

The yellow point represents the super master image acquisition date.

1.2.3. Phase unwrapping

Phase recovery is one of the most critical steps in displacement calculation processing. After calculating the interferometer, the obtained phase is ambiguous and changes in the interval $[-\pi, \pi]$. Phase recovery algorithms are utilized to convert this ambiguous phase to the real phase, a kind of integration method. It is mathematically impossible to solve. In this way, this problem solved by considering the Nyquist rate.

The SBAS algorithm described in [40]; [41] and [42] used to select the most suitable pixels for the time-series analysis and to calculate the LOS velocity of each pixel, with 50 as the number of best coherences interferograms threshold and 0.4 as the coherence threshold. The first threshold determines the minimal number of interferograms that might be utilized to calculate velocity, while the coherence threshold determines the pixels over which velocity can be calculated.

Based on results from prior research [43] and [38], phase unwrapping of interferograms was performed using a reference pixel placed in a stable location within the city. [44] used the Statistical-cost Network-flow Algorithm for Phase Unwrapping (SNAPHU) to individually unwrap coherent pixels within each

interferogram. The present paper's spatial phase was unwrapped prior to the stacking analysis. It was achieved utilizing the MCF phase unwrapping algorithm on a triangular irregular network.

1.2.4. Orbital refinement

This stage was primarily utilized to eliminate residual phases that did not fulfill the requirements and any ramp phases that remained after unwinding.

1.2.5. Retrieval of time series results

After unwrapping, the deformation phase was calculated using the singular value decomposition method, and the rate of deformation in each period was calculated. Finally, geocoding is utilized to retrieve the shape variable in each period's line-of-sight direction (LOS) (a negative value indicates a settlement, and a positive value indicates a lift).

1.3. Calculating of the vertical and horizontal displacements

Lake Urmia has been in a critical situation with decreased rainfall in recent years. Environmental changes have accompanied more groundwater abstraction and have led to subsidence in the area. The displacement values obtained from each set of descending or ascending images indicate line of sight (LOS) displacement. It is essential to calculate and separate displacement values into horizontal and vertical components to study various phenomena such as subsidence more accurately. So that movement in the satellite view direction may be separated into three primary components, north and east, by obtaining many images from multiple visual angles.

$$D_{LOS} = (-sin\theta cos\alpha \quad sin\theta sin\alpha \quad cos\theta)\begin{pmatrix} D_E \\ D_N \\ D_U \end{pmatrix} \qquad (1)$$

Where D_{LOS} is LOS displacement, θ is the incident angle, α is heading angle and D_E , D_N , D_U are respectively, displacement in the east, north, and vertical directions.

2. Result and Discussion

Figure 5 shows the mean velocity of displacement measured by the SBAS technology for both descending and ascending passes in the research area. The negative value of the deformation rate indicates subsidence, whereas the positive sign indicates a decreasing distance from the satellite with time (e.g., uplift). Figure 5 demonstrates this. The deformation velocity exceeds 210 mm/year in the LOS direction for descending the pass, and it is 91 mm/year for ascending the pass. In general, the subsidence on the bridge itself, especially its metal part, is considerable and high, but the subsidence in the initial and final parts of the bridge is less compared to the central parts.
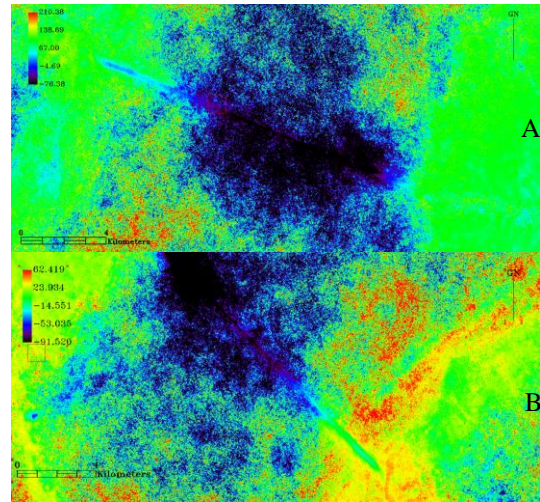

Figure 5. Mean Displacement-Velocity over the research area derived by SBAS technique for descending pass (A) and ascending pass (B)

The time-series displacements for both descending and ascending passes from November 2014 to April 2021 based on InSAR measurements over the research area at six locations are demonstrated in Figure 6.
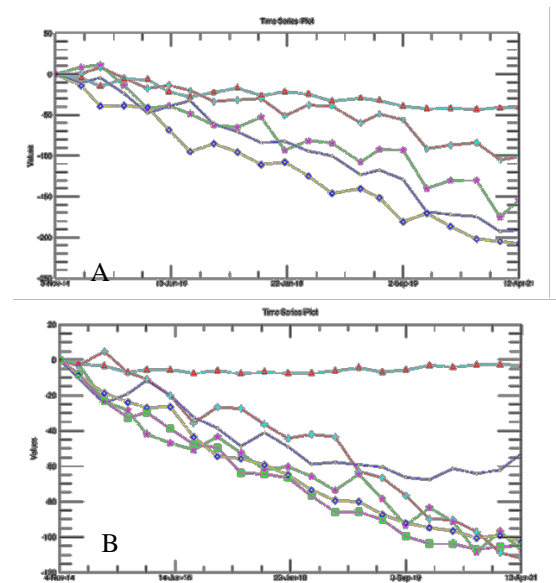

Figure 6. Time series subsidence of five points of Urmia Lake Bridge for Ascending pass (A) and six points of Urmia Lake Bridge for descending pass (B)

Central parts of the bridge have the most apparent subsidence, the annual subsidence rate exceeds 200 mm, and the maximum cumulative subsidence reaches 210 mm. However, the ground subsidence is relatively small and stable on both sides of the bridge. This study used data from the Urmia permanent GPS Station in the research area to compare GPS data with SBAS-InSAR processing products to evaluate the accuracy of SBAS-InSAR results based on Sentinel-1A data. The results include the horizontal and vertical displacements for ascending and descending passes, presented in Figure 7. Figure 7 shows that the GPS data agree with the SBAS-InSAR processing results.
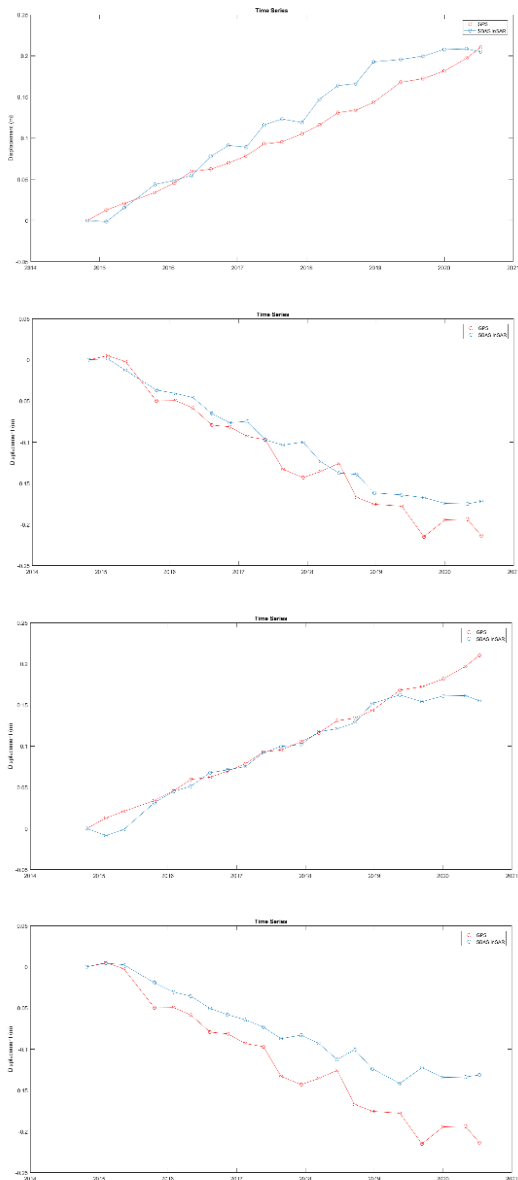
Figure 7. Comparison between SBAS InSAR- and GPS displacement time series of Urmia station (A) for horizontal directions in ascending pass, (B) vertical directions in ascending pass, (C) horizontal directions in descending the pass, and (D) vertical directions in descending pass

Two spectral angle errors and standard deviation criteria between the two methods were calculated to compare the two mentioned methods, and the results are shown in Table 1.

Table 1- Spectral angle error, standard deviation criteria between GPS results and SBAS InSAR results

	horizontal directions in ascending	vertical directions in ascending	horizontal directions in descending	vertical directions in descending
SAM (Radian)	0.5317	2.5912	0.5348	2.5701
RMSE (Meter)	0.0224	0.0218	0.0175	0.0453

The initial results show that the SBAS-InSAR approach is in good agreement with the GPS data, and the research findings are highly trustworthy. Both satellite orbit and the topographical data, tending to decrease InSAR precision, maybe overprinted with artifacts due to temporal changes to atmospheric time delays and mistakes. The SBAS approach enables us to minimize the atmosphere, baseline, and other artifacts efficiently. By this factor, InSAR measurement represents an annual (average) interferogram rate, while GPS measurement represents deformation observations between two periods of time. Thus, InSAR data will differ from GPS for places where time variable displacements occur.

3. Conclusion

The present paper uses the SBAS-InSAR technique to examine ground subsidence in the Urmia Lake Bridge Using 42-science Sentinel-1A data in descending and ascending passes. The research area's average subsidence rate and phase deformation information were acquired from November 2014 to April 2021. Compared to GPS data in the study area, the results demonstrate the validity of the SBAS-InSAR approach. According to SBAS-InSAR inversion results in the study area, ground subsidence will be severe on the bridge from 2014 to 2021. The highest total subsidence is 210 mm, and the yearly subsidence rate exceeds 200 mm. The deformation velocity surpasses 210 mm/year for descending pass and 91 mm/year for ascending the pass in the LOS direction. The main factors impacting surface deformation in Urmia Lake include overexploitation of groundwater and a decrease in rainfall, leading to an increase in the range and area of ground subsidence in the Urmia Lake Bridge.
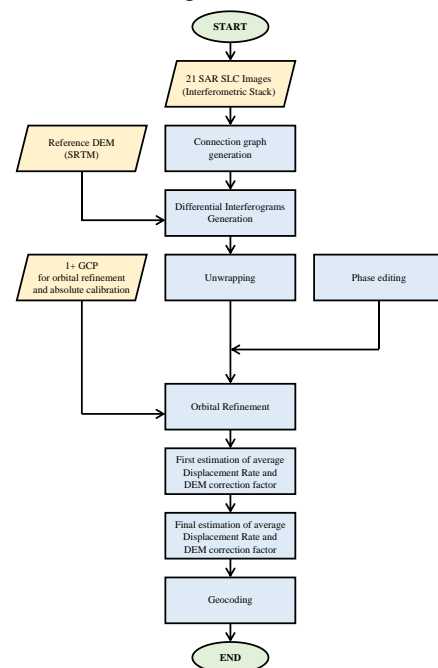

Figure 8. Flowchart data processing of SBAS

References

[1] Z. Du, L. Ge, X. Li, and A. Hay-Man Ng, "Subsidence monitoring over the Southern Coalfield, Australia using both L-Band and C-Band SAR time series analysis," *Remote Sens.*, vol. 8, no. 7, Jul. 2016, doi: 10.3390/RS8070543.

[2] L. Ge, A. H. Ng, X. Li, H. Z. Abidin, and I. Gumilar, "Remote Sensing of Environment Land subsidence characteristics of Bandung Basin as revealed by ENVISAT ASAR and ALOS PALSAR interferometry," *Remote Sens. Environ.*, vol. 154, pp. 46–60, 2014, doi: 10.1016/j.rse.2014.08.004.

[3] L. Zhou, J. Guo, J. Hu, J. Ma, F. Wei, and X. Xue, "Subsidence analysis of ELH Bridge through ground-based interferometric radar during the crossing of a subway shield tunnel underneath the bridge Subsidence analysis of ELH Bridge through ground-based," *Int. J. Remote Sens.*, vol. 39, no. 6, pp. 1911–1928, 2018, doi: 10.1080/01431161.2017.1416698.

[4] F. Qu, Q. Zhang, Z. Lu, C. Zhao, C. Yang, and J. Zhang, "Land subsidence and ground fissures in Xi'an, China 2005-2012 revealed by multi-band InSAR time-series analysis," *Remote Sens. Environ.*, vol. 155, pp. 366–376, 2014, doi: 10.1016/j.rse.2014.09.008.

[5] H. Yang and J. Peng, "Monitoring Urban Subsidence with Multi-master Radar Interferometry Based on Coherent Targets," 2015, doi: 10.1007/s12524-014-0434-0.

[6] D. GuangYao, G. HuiLi, L. Huanhuan, Z. Youquan, C. BeiBei, and L. KunChao, "Monitoring and Analysis of Land Subsidence Along Beijing-Tianjin Inter-City Railway," *J. Indian Soc. Remote Sens.*, vol. 44, no. 6, pp. 915–931, 2016, doi: 10.1007/s12524-016-0556-7.

[7] D. Massonnet and K. L. Feigl, "Radar interferometry and its application to changes in the earth's surface," *Rev. Geophys.*, vol. 36, no. 4, pp. 441–500, 1998, doi: 10.1029/97RG03139.

[8] F. Amelung, D. L. Galloway, J. W. Bell, H. A. Zebker, and R. J. Laczniak, "Sensing the ups and downs of Las Vegas: InSAR reveals structural control of land subsidence and aquifer-system deformation," *Geology*, vol. 27, no. 6, pp. 483–486, 1999, doi: 10.1130/0091-7613(1999)027<0483:STUADO>2.3.CO;2.

[9] D. Dzurisin, M. P. Poland, and R. Bürgmann, "Steady subsidence of Medicine Lake volcano, northern California, revealed by repeated leveling surveys," *J. Geophys. Res. Solid Earth*, vol. 107, no. B12, p. ECV 8-1-ECV 8-16, 2002, doi: 10.1029/2001jb000893.

[10] P. Baldi, G. Casula, N. Cenni, F. Loddo, and A. Pesci, "GPS-based monitoring of land subsidence in the Po Plain (Northern Italy)," *Earth Planet. Sci. Lett.*, vol. 288, no. 1–2, pp. 204–212, Oct. 2009, doi: 10.1016/J.EPSL.2009.09.023.

[11] E. Carminati and G. Martinelli, "Subsidence rates in the Po Plain, northern Italy: the relative impact of natural and anthropogenic causation," *Eng. Geol.*, vol. 66, no. 3–4, pp. 241–255, Nov. 2002, doi: 10.1016/S0013-7952(02)00031-5.

[12] I. Anell, H. Thybo, and I. M. Artemieva, "Cenozoic uplift and subsidence in the North Atlantic region: Geological evidence revisited," *Tectonophysics*, vol. 474, no. 1–2, pp. 78–105, Sep. 2009, doi: 10.1016/J.TECTO.2009.04.006.

[13] P. Psimoulis, M. Ghilardi, E. Fouache, and S. Stiros, "Subsidence and evolution of the Thessaloniki plain, Greece, based on historical leveling and GPS data," *Eng. Geol.*, vol. 90, no. 1–2, pp. 55–70, Mar. 2007, doi: 10.1016/J.ENGGEO.2006.12.001.

[14] H. Sun, Q. Zhang, C. Zhao, C. Yang, Q. Sun, and W. Chen, "Monitoring land subsidence in the southern part of the lower Liaohe plain, China with a multi-track PS-InSAR technique," *Remote Sens. Environ.*, vol. 188, no. January, pp. 73–84, 2017, doi: 10.1016/j.rse.2016.10.037.

[15] O. Mora, J. J. Mallorqui, and A. Broquetas, "Linear and nonlinear terrain deformation maps from a reduced set of interferometric SAR images," *IEEE Trans. Geosci. Remote Sens.*, vol. 41, no. 10 PART I, pp. 2243–2253, 2003, doi: 10.1109/TGRS.2003.814657.

[16] L. Ji, Y. Zhang, Q. Wang, Y. Xin, and J. Li, "Detecting land uplift associated with enhanced oil recovery using InSAR in the Karamay oil field, Xinjiang, China," *Int. J. Remote Sens.*, vol. 37, no. 7, pp. 1527–1540, 2016, doi: 10.1080/01431161.2016.1154222.

[17] J. K. Hole, C. J. Bromley, N. F. Stevens, and G. Wadge, "Subsidence in the geothermal fields of the Taupo Volcanic Zone, New Zealand from 1996 to 2005 measured by InSAR," *J. Volcanol. Geotherm. Res.*, vol. 166, no. 3–4, pp. 125–146, 2007, doi: 10.1016/j.jvolgeores.2007.07.013.

[18] V. Tofani, F. Raspini, F. Catani, and N. Casagli, "Persistent scatterer interferometry (psi) technique for landslide characterization and monitoring," *Remote Sens.*, vol. 5, no. 3, pp. 1045–1065, 2013, doi: 10.3390/rs5031045.

[19]   A. Rateb and A. Z. Abotalib, "Inferencing the land subsidence in the Nile Delta using Sentinel-1 satellites and GPS between 2015 and 2019," *Sci. Total Environ.*, vol. 729, p. 138868, 2020, doi: 10.1016/j.scitotenv.2020.138868.

[20]   B. Li, Z. Wang, J. An, C. Zhou, and Y. Ma, "Time-Series Analysis of Subsidence in Nanning, China, Based on Sentinel-1A Data by the SBAS InSAR Method," *PFG - J. Photogramm. Remote Sens. Geoinf. Sci.*, vol. 88, no. 3–4, pp. 291–304, 2020, doi: 10.1007/s41064-020-00118-9.

[21]   P. Blanco-Sánchez, J. J. Mallorquí, S. Duque, and D. Monells, "The coherent pixels technique (CPT): An advanced DInSAR technique for nonlinear deformation monitoring," *Pure Appl. Geophys.*, vol. 165, no. 6, pp. 1167–1193, 2008, doi: 10.1007/s00024-008-0352-6.

[22]   C. Werner, U. Wegmüller, T. Strozzi, and A. Wiesmann, "Interferometric Point Target Analysis for Deformation Mapping," *Int. Geosci. Remote Sens. Symp.*, vol. 7, no. 1, pp. 4362–4364, 2003, doi: 10.1109/igarss.2003.1295516.

[23]   G. Aslan, M. Foumelis, D. Raucoules, M. De Michele, S. Bernardie, and Z. Cakir, "Landslide mapping and monitoring using persistent scatterer interferometry (PSI) technique in the French alps," *Remote Sens.*, vol. 12, no. 8, 2020, doi: 10.3390/RS12081305.

[24]   J. M. D. Blasco, M. Foumelis, C. Stewart, and A. Hooper, "Measuring urban subsidence in the Rome Metropolitan Area (Italy) with Sentinel-1 SNAP-StaMPS Persistent Scatterer Interferometry," *Remote Sens.*, vol. 11, no. 2, pp. 1–17, 2019, doi: 10.3390/rs11020129.

[25]   B. Hu, B. Yang, X. Zhang, X. Chen, and Y. Wu, "Time-series displacement of land subsidence in fuzhou downtown, monitored by SBAS-InSAR Technique," *J. Sensors*, vol. 2019, 2019, doi: 10.1155/2019/3162652.

[26]   Z. Kui, A. Hay-Man Ng, L. Ge, Y. Dong, and C. Rizos, "Multi-path palsar interferometric observations of the 2008 magnitude 8.0 Wenchuan Earthquake," *Int. J. Remote Sens.*, vol. 31, no. 13, pp. 3449–3463, 2010, doi: 10.1080/01431161003727804.

[27]   E. Gebremichael, M. Sultan, R. Becker, M. El Bastawesy, O. Cherif, and M. Emil, "Assessing Land Deformation and Sea Encroachment in the Nile Delta: A Radar Interferometric and Inundation Modeling Approach," *J. Geophys. Res. Solid Earth*, vol. 123, no. 4, pp. 3208–3224, 2018, doi: 10.1002/2017JB015084.

[28]   G. Wöppelmann *et al.*, "Is land subsidence increasing the exposure to sea level rise in Alexandria, Egypt?," *Geophys. Res. Lett.*, vol. 40, no. 12, pp. 2953–2957, 2013, doi: 10.1002/grl.50568.

[29]   D. Tapete, N. Casagli, G. Luzi, R. Fanti, G. Gigli, and D. Leva, "Integrating radar and laser-based remote sensing techniques for monitoring structural deformation of archaeological monuments," *J. Archaeol. Sci.*, vol. 40, no. 1, pp. 176–189, 2013, doi: 10.1016/j.jas.2012.07.024.

[30]   L. Hui, C. Fulong, and Z. Qing, "Land deformation monitoring using coherent target-neighbourhood networking method combined with polarimetric information: A case study of Shanghai, China," *Int. J. Remote Sens.*, vol. 32, no. 9, pp. 2395–2407, 2011, doi: 10.1080/01431161003698328.

[31]   P. Berardino, G. Fornaro, R. Lanari, S. Member, E. Sansosti, and S. Member, "A New Algorithm for Surface Deformation Monitoring Based on Small Baseline Differential SAR Interferograms," vol. 40, no. 11, pp. 2375–2383, 2002.

[32]   O. Mora, "A Small-Baseline Approach for Investigating Deformations on Full-Resolution Differential SAR Interferograms," no. August, 2004, doi: 10.1109/TGRS.2004.828196.

[33]   U. Wegmüller, S. Member, D. Walter, V. Spreckels, C. L. Werner, and S. Member, "Nonuniform Ground Motion Monitoring With TerraSAR-X Persistent Scatterer Interferometry," vol. 48, no. 2, pp. 895–904, 2010.

[34]   X. Lu and X. Sun, "Ground Subsidence Monitoring in Cheng Du Plain Using DInSAR SBAS Algorithm," vol. 1, pp. 535–545, 2017, doi: 10.1007/978-981-10-3966-9.

[35]   M. Guizar-sicaaros, S. T. Thurman, and J. R. Fienup, "Efficient subpixel image registration algorithms," vol. 33, no. 2, pp. 156–158, 2008.

[36]   B. Hu, H. S. Wang, Y. L. Sun, J. G. Hou, and J. Liang, "Long-term land subsidence monitoring of Beijing (China) using the small baseline subset (SBAS) technique," *Remote Sens.*, vol. 6, no. 5, pp. 3648–3661, 2014, doi: 10.3390/rs6053648.

[37]   L. Zhoua, J. Guo, J. Hu, J. Ma, F. Wei, and X. Xue, "Subsidence analysis of ELH bridge through ground-based interferometric radar during the crossing of a subway shield tunnel underneath the bridge," *Int. J. Remote Sens.*, vol. 39, no. 6, pp. 1911–1928, 2018, doi: 10.1080/01431161.2017.1416698.

[38]   Y. Yan *et al.*, "Mexico City Subsidence Measured by InSAR Time Series : Joint Analysis Using PS and SBAS Approaches," vol. 5, no. 4, pp. 1312–1326, 2012.

[39] D. Type and T. Note, "Sentinel-1 Instrument Processing Facility : Impact of the Elevation Antenna Pattern Phase," no. 22, pp. 1–15, 2015.

[40] A. Sowter, L. Bateson, P. Strange, K. Ambrose, and M. F. Syafiudin, "DInSAR estimation of land motion using intermittent coherence with application to the South Derbyshire and Leicestershire coalfields," no. November 2014, pp. 37–41, 2013, doi: 10.1080/2150704X.2013.823673.

[41] L. Bateson, F. Cigna, D. Boon, and A. Sowter, "International Journal of Applied Earth Observation and Geoinformation The application of the Intermittent SBAS (ISBAS) InSAR method to the South Wales Coalfield , UK," *Int. J. Appl. Earth Obs. Geoinf.*, vol. 34, pp. 249–257, 2015, doi: 10.1016/j.jag.2014.08.018.

[42] F. Cigna *et al.*, "Intermittent Small Baseline Subset (ISBAS) monitoring of land covers unfavourable for conventional C-band InSAR : proof-of-concept for peatland environments in north Wales , UK," vol. 9243, pp. 1–6, 2014, doi: 10.1117/12.2067604.

[43] B. Osmano, "Article in press," 2010, doi: 10.1016/j.jag.2010.05.009.

[44] C. W. Chen and H. A. Zebker, "of statistical models for cost functions in nonlinear optimization," vol. 18, no. 2, pp. 338–351, 2001.